# Evaluation of [$^{13}$N]ammonia Positron Emission Tomography for Quantifying Glutamine Synthetase Activity in the Human Brain.

**Alice Egerton** ( Alice.Egerton@kcl.ac.uk )
https://orcid.org/0000-0003-2939-064X
**Joel Dunn**
King's College London
**Nisha Singh**
King's College London
**Zilin Yu**
King's College London
**Jim O'Doherty**
King's College London
**Ivan Koychev**
King's College London
**Jessica Webb**
King's College London
**Simon Claridge**
King's College London
**Federico Turkheimer**
King's College London
**Paul Marsden**
King's College London
**Alexander Hammers**
King's College London
**Antony Gee**
King's College London

**Original research**

**Keywords:** Glutamate, glutamine, glutamate turnover, positron emission tomography, ammonia

**Posted Date:** May 27th, 2020

**DOI:** https://doi.org/10.21203/rs.3.rs-29881/v1



**Version of Record:** A version of this preprint was published at EJNMMI Research on December 3rd, 2020. See the published version at https://doi.org/10.1186/s13550-020-00731-0.

# Abstract

**Purpose** The conversion of synaptic glutamate to glutamine in astrocytes by glutamine synthetase (GS) is critical to maintaining healthy brain activity and may be disrupted in several brain disorders. As the GS catalysed conversion of glutamate to glutamine requires ammonia, we evaluated whether [$^{13}$N]ammonia positron emission tomography (PET) could reliability quantify GS activity in humans.

**Methods** In this test-retest study, eight healthy volunteers each received two dynamic [$^{13}$N]ammonia PET scans on the morning and afternoon of the same day. Each [$^{13}$N]ammonia scan was preceded by a [$^{15}$O]water PET scan to account for effects of cerebral blood flow (CBF).

**Results** Concentrations of radioactive metabolites in arterial blood were available for both sessions in five of the eight subjects. Our results demonstrated that kinetic modelling was unable to reliably distinguish estimates of the kinetic rate constant $k_3$ (related to GS activity) from $K_1$ (related to [$^{13}$N]ammonia brain uptake), and indicated a non-negligible back-flux of [$^{13}$N]ammonia to blood ($k_2$). Model selection favoured a reversible one tissue compartmental model, and [$^{13}$N]ammonia $K_1$ correlated reliably ($r^2$ = 0.72–0.92) with [$^{15}$O]water CBF.

**Conclusion** The [$^{13}$N]ammonia PET method was unable to reliably estimate GS activity in the human brain but may provide an alternative index of CBF.


# Introduction

The metabolism of glutamate to glutamine by the enzyme glutamine synthetase (GS) is a key process for maintaining healthy synaptic function. GS (encoded by the gene glutamate-ammonia ligase, Glul) is predominantly expressed in astrocytes [1] and converts glutamate released into the synapse during neurotransmission to glutamine, for recycling to neuronal glutamate and gamma-amino butyric acid (GABA). GS is therefore critical to the homeostasis of excitatory and inhibitory neurotransmission and normal brain activity [2, 3]. This process may be compromised in several brain disorders [3], and neuroimaging techniques to assess GS activity *in vivo* could have wide-ranging research or clinical impact.

Abnormalities in GS have been most clearly linked to epileptogenesis [4]. Very rare inherited deficits in GS are associated with neonatal seizures [5, 6]. Pharmacological inhibition of GS [2] or genetic GS deficiency [7] can be used as animal models of epilepsy, and there are marked reductions in GS in areas of hippocampal tissue resected from patients with mesial temporal lobe epilepsy [8, 9]. Furthermore, regional differences in the level of GS protein, mRNA expression or activity have been detected in post-mortem brain tissue across many psychiatric and neurological disorders. The results of these studies, summarised in Supplementary Table 1, suggest that in addition to applications in epilepsy, GS imaging could be important in understanding or predicting schizophrenia, depression or suicidal behaviour, amongst other disorders.

GS is also the main pathway for metabolism of brain ammonia, which is required for the conversion of glutamate of glutamine [10]. This raises the possibility that radiolabelled ammonia in combination with positron emission tomography (PET) may be utilised to measure brain GS activity. [$^{13}$N]Ammonia PET is used clinically to assess myocardial perfusion (”blood flow”) and has been applied in research studies examining abnormalities in brain ammonia uptake associated with liver disease [11–20] and in the diagnosis of brain tumours [21].

The aim of this study was to evaluate [$^{13}$N]ammonia as a PET tracer for quantification of brain GS activity. This evaluation requires kinetic modelling of the dynamic concentrations of $^{13}$N-derived radioactivity in the brain and arterial blood following radiotracer injection, in an attempt to reliably extract rate constants indexing GS activity, as the rate of conversion of [$^{13}$N]ammonia to [$^{13}$N]glutamine, from the signal relating to [$^{13}$N]ammonia brain uptake and clearance (see Supplement Fig. 1). To do this we sought to acquire two [$^{13}$N]ammonia scans (test and re-test) in eight healthy volunteers. In order to

account for effects of cerebral blood flow (CBF), we additionally acquired test and re-test [$^{15}$O]water PET scans in the same subjects on the same day, with [$^{15}$O]water PET scans preceding [$^{13}$N]ammonia PET.

## Methods

The study had ethical approval from the NHS Ethical Committee (NRES South East Coast, Surrey), the local Research and Development offices and the Administration of Radioactive Substances Advisory Committee (ARSAC). Participation required provision of written informed consent to all study procedures.

# Participants

The study aimed to acquire complete datasets (including one T1-weighted MRI scan, two [$^{13}$N]ammonia scans and two [$^{15}$O]water PET scans) in eight healthy volunteers. Participants were recruited internally though King's College London's recruitment system. Inclusion required that participants were aged 18 or older and were able to provide written informed consent in English. Exclusion criteria included the standard contraindications to PET and MRI, including pregnancy. Absence of pregnancy in female participants was confirmed by a negative urine pregnancy test on arrival to the PET scanning visit.

# MRI

MRI scans were performed at the Centre for Neuroimaging Sciences, King's College London, UK on a General Electric MR750 3 T MRI scanner. A T1-weighted structural MRI scan based on the ADNI protocol (voxel size 1.05 × 1.05 × 1.20 mm, TE 3.016 ms; TR 7.312 ms matrix 256 × 256; FoV 270 mm; inversion time 400 ms) was acquired for co-registration of the participants' PET images.

# Radiochemistry

Aqueous [$^{13}$N]$NH_3$ was produced on a CTI RDS 112 biomedical cyclotron via the $^{16}O(p,\alpha)^{13}N$ nuclear reaction. The target contained 8 mL $H_2O$ with 5 mM ethanol according to Wieland et al [22].

[$^{15}$O]water: Oxygen-15 was produced in the form of [$^{15}$O]oxygen gas by the bombardment of enriched [$^{15}$N]nitrogen gas containing 1-2.5% oxygen gas via the $^{15}N(p,n)^{16}0$ nuclear reaction. [$^{15}$O]water was subsequently obtained by passage with hydrogen over a platinum catalyst according to Berridge et al [23].

# PET image acquisition

PET scans were acquired at St Thomas' Hospital, King's College London on a GE Discovery 710 PET-CT scanner with 3D acquisition and list mode. Each participant underwent two PET scanning sessions, performed in the morning and afternoon of the same day. Each of the two scanning sessions consisted of an initial low dose CT scan to enable correction for tissue attenuation of radioactivity, a dynamic [$^{15}$O]water scan (5 minutes), and a dynamic [$^{13}$N]ammonia scan (30 minutes). There was a break of approximately one hour between the two sessions, during which lunch was provided, and an appropriate gap (at least 5 half-lives) between subsequent scans to avoid residual counts (i.e. at least 10 minutes following the [$^{15}$O]water scans and 50 minutes following the [$^{13}$N]ammonia scan) .

At the start of the PET scan visit, a cannula was inserted in a vein in the arm for radiotracer injection. After application of local anaesthetic, an arterial line was inserted into the radial artery and flushed every 20 minutes with heparinised saline (20 IU/mL of heparin in sterile 0.9% *w/v* sodium chloride) until removal at the end of PET scanning. Just before the start of each scanning session, 6 mL of arterial blood was taken to measure baseline blood ammonia levels.

Participants were positioned in the PET-CT scanner, with head movement minimised via a moulded headrest and head strap. The arterial line was connected to an automated blood sampling system (Allogg ABSS, www.allogg.se, Sweden). CT scout (0.05 mSv) scans were acquired. $^{15}$O-water (target dose at time of administration:

960 MBq, 1.10 mSv) was injected through the venous cannula over 10 seconds. PET image acquisition started 10 seconds before the start of [$^{15}$O]water injection and continued for a total of 5 minutes. Arterial blood collection via the fluid analyser commenced 70 seconds before [$^{15}$O]water injection and 60 seconds before the start of scan acquisition and continued for the 5 minute scan duration, to a total of 25 mL. Additionally, a single 2 mL arterial blood sample was manually drawn at 3 minutes into the scan.

After completion of the [$^{15}$O]water scan the arterial line was flushed with heparinised saline. At least 20 minutes after the end of the $^{15}$O-water scan (25 minutes after [$^{15}$O]water injection), [$^{13}$N]ammonia (target dose at time of administration: 550 MBq, 1.5 mSv) was injected through the venous cannula. PET image acquisition started 10 seconds before the start of [$^{13}$N]ammonia injection and continued for 30 minutes. Arterial blood collection via the fluid analyser commenced 70 seconds before [$^{13}$N]ammonia injection and 60 seconds before the start of scan acquisition and continued for 15 minutes, to a total of 75 mL. In addition, 6 manual arterial blood samples of 10 mL each were drawn at 5-minute intervals during the [$^{13}$N]ammonia scans.

In the second session, a minimum of one hour later, both the [$^{15}$O]water and [$^{13}$N]ammonia scans were repeated using identical acquisition protocols.

# Ammonia and metabolite analysis

Levels of non-radioactive ammonia in arterial blood were determined from samples collected before radiotracer collection. These samples were collected in K-EDTA tubes (pre-tested and confirmed as ammonia-free) and transported on ice within 20 minutes of collection to the hospital laboratory for standard analysis.

Unless stated otherwise, all water used in these metabolite analyses was passed through ion exchange resin and 0.22 μm membrane filtered to produce water with a specific resistance of 18.2 micro-ohms using a Milli-Q Ultrapure water purification system manufactured by Millipore Corporation.

Plasma was separated from whole blood by centrifuging at 3000 x *g* for 3 minutes at room temperature (RT). Levels of radioactive metabolites in plasma were estimated through solid phase extraction, based on the methods of Keiding et al.[17] In preparation for solid phase extraction, one cartridge was filled with 0.6 mL Dowex 1 × 8–50 anion exchange resin and pre-treated with 6 mL 0.75 M sodium acetate solution. A second cartridge, connected in series via an Agilent Bond Elut adapter, was filled with 0.35 mL AG50W-X8 cation exchange resin and pretreated with 3.5 mL 0.8 M Tris-acetate solution. The third cartridge which connected to second cartridge in same way via adapter was filled with 0.35 mL AG50W-X8 cation exchange resin and pretreated with 3.5 mL Milipore water.

For extraction, 0.5 mL of the supernatant protein-free plasma was loaded onto the first cartridge followed by washing with 3 mL of Milipore water through the cartridge stack and flushed with 10 mL of air. The eluent from the first cartridge passed through second cartridge and third cartridge, which were subsequently washed with 7 mL of Milipore water followed by 10 mL of air. The third cartridge was washed with 7 ml Milipore water and followed by 10 mL of air. All eluate were collected with a 25 mL pot. With this method, the radioactivity measured on the first cartridge corresponded to [13N]glutamate, on the second cartridge corresponded to intact [13N]ammonia, on the third cartridge corresponded to [13N]glutamine, and the pot corresponded to [13N]urea .

A 10-detector gamma-counter (Wizard2 2470, Perkin-Elmer) cross-calibrated to the PET scanner was used to measure radioactivity concentrations in whole blood (0.5 mL per sample), plasma (0.5 mL per sample) and metabolite fractions (3 mL for urea and full cartridge contents for other fractions). All samples were counted for 3 minutes on a fixed energy window (358–664 keV) with software cross-talk correction and in-house volumetric geometry correction. The samples and cartridges were corrected for weight to calculate the total radioactivity of blood sample analysed.

# Image processing

[$^{15}$O]water PET list mode data was unlisted to 26 frames (1 × 10 sec, 10 x sec, 6 × 10 sec and 9 × 20 sec). [$^{13}$N]$NH_3$ PET list mode was unlisted to 47 frames (1 × 10 sec, 10 × 5 sec, 6 × 10 sec, 3 × 20 sec, 27 × 60 sec). All PET images were reconstructed to 256 matrix with 47 slices with 0.98 × 0.98 × 3.27 mm voxel size, 3D iterative reconstruction and decay correction. Images were reconstructed with CT attenuation correction (attenuation corrected, AC) and without (non-attenuation corrected, NAC).

Frame-by-frame motion correction was performed on dynamic PET data using the NAC image to derive the rigid-body motion parameters. Regions of interest (ROI) were defined by the "Hammers_mith Atlas" [24, 25] (83 regions) in MNI stereotaxic space. Non-linear warps from MNI to subject space were defined using the unified segmentation algorithm [26] in SPM8 (www.fil.ucl.ac.uk/spm) on each subject's T1 MRI. Resliced atlases for each subject were then co-registered to a summed PET image for each PET scan via the MRI.

# Kinetic analysis

For both the [$^{15}$O]water and [$^{13}$N]ammonia scans, time activity curves (TACs) were extracted from the co-registered Hammers_mith atlas [24, 25]. Using each subject's co-registered probabilistic grey matter mask from the segmented MRI, TAC's were extracted using the mean voxel value within the region, or a weighted mean for cortical regions. This resulted in values from 77 individual ROI's. A whole-brain grey matter weighted mean TAC was also defined Ventricular and white matter regions were ignored.

For the [$^{13}$N]ammonia scans, arterial whole blood input functions were created from decay-corrected continuous blood samples with manual samples used for cross-calibration to scanner and interpolation to scan end. Plasma-over-blood ratio was calculated as the mean of the manual sample ratios for each subject. Parent fraction data (ratio of [$^{13}$N]ammonia to total $^{13}$N activity) was fitted to a biexponential curve for each subject.[11] A population parent fraction function was created by fitting a biexponential curve to all subject data. Parent plasma input functions (i.e. [$^{13}$N]ammonia in plasma only) for the kinetic modelling were created by multiplying the whole-blood input function by plasma-over-blood ratios and the biexponential curve fitted to the parent fractions. Whole blood and parent plasma input functions were delay corrected by visually matching the blood rise with the grey matter TAC, with appropriate decay correction.

Regional cerebral blood flow (CBF) was calculated from the [$^{15}$O]water TACs using a 5- parameter free diffusion model [27]. In brief, a nonlinear least squares fit method was used to estimate the 5 parameters of this 1-tissue compartment model: $K_1$ (CBF), $k_2$ (wash-out), blood fraction, and delay and dispersion of the blood curve between the brain and sampling point.

Ammonia is a freely diffusible tracer and as such has been used to quantify perfusion in myocardium[28] and brain.[29] Though ammonia is rapidly trapped in tissue, in order to index GS activity, the kinetic parameters describing the uptake of [$^{13}$N]ammonia by GS must be distinguishable from those reflecting CBF. The model chosen for primary analysis of [$^{13}$N]ammonia scans was an irreversible two tissue compartment model (2TCM) as used in Keiding et al., 2006 [11]. To confirm the model choice a nonlinear spectral analysis approach was used to identify the most appropriate tissue uptake model [30]. In brief, the data was fitted to a number of candidate PET compartmental models with increasing numbers of parameters. In this case, a reversible 2TCM [Supplement Fig. 1] was the most complex model considered, with increasingly simpler models defined by setting $k_4$, $k_3$, $k_2$ to zero (i.e. 4 candidate models). The blood fraction contributing to the TAC for each region was also included as a free parameter.

Each compartmental model was fitted using a weighted least squares method with residual weights for each frame determined by frame duration and radioactive decay: $\sqrt{\left(\Delta_i e^{-\lambda t_i}\right)}$, where $\lambda$ is the decay rate constant, and $\Delta_i$ and $t_i$ are the frame duration and frame mid-point time respectively for frame $i$. Model fit was assessed using the Akaike Information Criterion.[31]

Additional macroparameters from the $^{15}$O and $^{13}$N scans were calculated to compare with the results of Keiding et al (2006) urface area product of the blood brain barrier to [$^{13}$N]ammonia) was calculated

as

$$PS_{BBB} = -CBF\ln(1 - K_1 / CBF)$$

where CBF is calculated from the [$^{15}$O]water scan, and $K_1$ from the [$^{13}$N]ammonia scan. Net metabolic clearance of [$^{13}$N]ammonia in blood into intracellular [$^{13}$N]glutamine, $K_{met}$, was calculated using the Patlak graphical method [32]. $PS_{met}$ (flow-independent permeability-surface area product of conversion of ammonia to intracellular glutamine) was calculated as

$$PS_{met} = -CBF\ln(1 - K_{met}/ CBF)$$

Finally, the cerebral metabolic rate of ammonia, CMRA, was calculated as

$$CMRA = K_{met}A$$

where A is the measured concentration of endogenous ammonia in the blood.

Kinetic parameter repeatability between the test-retest scans was assessed using mean fractional difference (VAR), absolute fractional difference (AbsVAR), and intraclass correlation coefficient (ICC) using a two-way random model for consistency [33]. For 8 subjects, the threshold for a significantly positive ICC is 0.58 at the at the $p < 0.05$ level. VAR and AbsVAR were calculated for N subjects as a percentage:

$$VAR = \frac{1}{N}\sum_{i=1}^{N} 200 \times \frac{retestValue_i - testValue_i}{testValue_i + retestValue_i}$$

$$AbsVAR = \frac{1}{N}\sum_{i=1}^{N} 200 \times \frac{|testValue_i - retestValue_i|}{testValue_i + retestValue_i}$$

Image registration, TAC extraction, blood data processing, kinetic modeling and statistical analyses were performed in Matlab (www.mathworks.com). Data are presented as mean ± s.d. unless otherwise stated.

## Results

# Participants

Eight volunteers (3 female) underwent all PET-CT and MRI scans. Age at scan was 25.0 ± 2.5 years. Weight, height and BMI were 75.7 ± 9.3 kg, 1.74 ± 0.13 m and 25.3 ± 4.1 kg/m$^2$ respectively.

# Scan parameters

Ammonia blood levels immediately prior to scan session one were 24.5 ± 5.7 μmol/L and prior to session two 23.9 ± 4.8 μmol/L. No significant difference was found between scan session within-subject (0.6 ± 7.9 μmol/L; range − 12.0–11.0). No significant differences were observed for the administered [$^{15}$O]water (mean ± SD = 841 ± 126 MBq, and 834 ± 146 MBq for sessions one and two, respectively) or the [$^{13}$N]ammonia (mean + SD = 537 ± 7 MBq and 537 ± 3 MBq for sessions one and two, respectively). Additionally, no significant differences were observed between the timings between sessions one and two. The mean time between [$^{15}$O]water and [$^{13}$N]ammonia injections was 48 ± 6 minutes and 46 ± 4 minutes for sessions one and two, respectively, with a minimum gap of 37 minutes. The mean time between first [$^{13}$N]ammonia and second [$^{15}$O]water injections was 88 ± 33 minutes (minimum 65 minutes).

# Kinetic Analysis and Repeatability: [$^{15}$O]Water

Visual inspection indicated that grey matter TAC fits were excellent (Supplement Fig. 2) and grey matter CBF was 37.6 ± 4.8 [illegible]e and two respectively (Table 1, no significant difference). Repeatability of CBF

calculations across 8 subjects was moderate (Table 2) and ICC values were significantly > 0 in 44 of 77 individual ROIs (mean ICC = 0.58 ± 0.23), but not in the whole brain grey matter TACs (ICC = 0.50). VAR and AbsVAR were 2.7% and 8.6% respectively for grey matter. Across individual ROIs, the mean ± s.d. values for VAR and AbsVAR were 2.3 ± 2.5% and 9.7 ± 2.5%, with values below 10% in 50 of 77 ROIs.

Table 1

Model parameters for test (S1) & retest (S2) scans for grey matter and selected regions of interest (ROIs). The table presents estimates of cerebral blood flow (CBF) from [$^{15}$O]water scans, and irreversible two tissue compartmental model parameter estimates for rate constants $K_1$, $k_2$ and $k_3$ from [$^{13}$N]ammonia scans. Data are presented as mean ± standard deviation for grey matter and the left (l) lingual gyrus (OL_ling_G), posterior cingulate gyrus (G_cing_post), putamen, thalamus, and cerebellum.

| | [$^{15}$O]water [n = 8] | | [$^{13}$N]ammonia [n = 5] | | | | | |
|---|---|---|---|---|---|---|---|---|
| ROI | CBF (ml/100 g/min) | | $K_1$ (ml/100 g/min) | | $k_2$ (1/min) | | $k_3$ (1/min) | |
| | S1 | S2 | S1 | S2 | S1 | S2 | S1 | S2 |
| Grey Matter | 37.6 ± 4.8 | 38.5 ± 3.4 | 20.1 ± 1.5 | 18.7 ± 1.3 | 0.0072 ± 0.0035 | 0.0096 ± 0.0042 | 0.0031 ± 0.0045 | 0.0177 ± 0.0259 |
| OL_ling_G_l | 40.8 ± 5.4 | 41.5 ± 2.8 | 23.7 ± 3.0 | 21.6 ± 0.9 | 0.0072 ± 0.0023 | 0.0090 ± 0.0035 | 0.0000 ± 0.0000 | 0.0125 ± 0.0172 |
| G_cing_post_l | 43.6 ± 5.3 | 44.3 ± 4.2 | 22.2 ± 1.6 | 20.8 ± 1.3 | 0.0069 ± 0.0038 | 0.0099 ± 0.0059 | 0.0038 ± 0.0052 | 0.0154 ± 0.0231 |
| Putamen_l | 45.3 ± 7.3 | 46.1 ± 5.5 | 23.3 ± 1.9 | 21.2 ± 1.5 | 0.0063 ± 0.0028 | 0.0086 ± 0.0037 | 0.0000 ± 0.0000 | 0.0144 ± 0.0203 |
| Thalamus_l | 43.9 ± 5.5 | 44.5 ± 4.2 | 22.8 ± 2.4 | 21.2 ± 1.2 | 0.0128 ± 0.0057 | 0.0178 ± 0.0075 | 0.0241 ± 0.0214 | 0.0405 ± 0.0234 |
| Cerebellum_l | 41.7 ± 6.8 | 42.6 ± 5.2 | 22.5 ± 2.0 | 20.7 ± 1.3 | 0.0070 ± 0.0047 | 0.0088 ± 0.0034 | 0.0056 ± 0.0126 | 0.0145 ± 0.0216 |

Table 2

Repeatability metrics for [$^{15}$O]water cerebral blood flow (CBF) and [$^{13}$N]ammonia two tissue compartment model parameters for grey matter and selected regions of interest (ROIs). The table presents the intraclass correlation coefficient (ICC), percent mean fractional difference (VAR) and percent absolute fractional difference (AbsVAR) across test and retest scans. Data are presented as mean ± standard deviation for grey matter and the left (l) lingual gyrus (OL_ling_G), posterior cingulate gyrus (G_cing_post), putamen, thalamus and cerebellum.

| | [$^{15}$O]water [n = 8] | | | [$^{13}$N]ammonia [n = 5] | | | | | | | | |
|---|---|---|---|---|---|---|---|---|---|---|---|---|
| ROI | CBF | | | $K_1$ | | | $k_2$ | | | $k_3$ | | |
| | ICC | VAR | AbsVAR | ICC | VAR | AbsVAR | ICC | VAR | AbsVAR | ICC | VAR | AbsVAR |
| Grey Matter | 0.50 | 3 ± 11 | 9 ± 6 | -0.79 | -7 ± 13 | 10 ± 11 | 0.94 | 29 ± 18 | 29 ± 18 | 0.02 | -30 ± 179 | 153 ± 62 |
| OL_ling_G_l | 0.22 | 2 ± 13 | 10 ± 9 | -0.42 | -8 ± 15 | 10 ± 14 | 0.86 | 21 ± 13 | 21 ± 13 | -0.00 | 71 ± 165 | 147 ± 80 |
| G_cing_post_l | 0.68 | 2 ± 9 | 8 ± 4 | -0.78 | -7 ± 13 | 9 ± 11 | 0.86 | 34 ± 24 | 34 ± 24 | 0.15 | 13 ± 196 | 173 ± 37 |
| Putamen_l | 0.85 | 2 ± 8 | 7 ± 2 | -0.84 | -9 ± 14 | 12 ± 12 | 0.85 | 31 ± 24 | 31 ± 24 | -0.00 | 59 ± 194 | 181 ± 33 |
| Thalamus_l | 0.66 | 2 ± 9 | 7 ± 5 | -0.64 | -7 ± 15 | 11 ± 11 | 0.76 | 35 ± 27 | 37 ± 25 | 0.42 | 80 ± 95 | 105 ± 57 |
| Cerebellum_l | 0.69 | 3 ± 12 | 9 ± 7 | -0.58 | -8 ± 13 | 9 ± 13 | 0.91 | 30 ± 27 | 32 ± 24 | 0.22 | -58 ± 157 | 138 ± 73 |

# Kinetic Analysis and Repeatability: [$^{13}$N]Ammonia

Continuous and manual blood sampling was obtained for all scans in all 8 subjects. [$^{13}$N]ammonia and [$^{13}$N]metabolite fractions were successfully obtained for five subjects but failed in three subjects due to issues with later preparation of solid phase extraction materials. In the successful 5 subjects, biexponential curve fits to parent fractions were in line with results from Keiding et al[11] (Fig. 1). Data from these 5 subjects were used to determine the [$^{13}$N]ammonia kinetic model parameter fits and repeatability.

[$^{13}$N]ammonia PET images showed regional variation in signal intensity, with highest uptake in the occipital lobes, posterior cingulate gyri, putamina, thalami and cerebella Table 1 presents $K_1$, $k_2$ & $k_3$ values for the [$^{13}$N]ammonia scans from subjects 1–5, calculated using the irreversible 2TCM across grey matter and in selected high uptake ROI in the left hemisphere. $K_1$ values were comparable between subjects and scan sessions. $K_1$ ICC values (Table 2) were negative indicating poor within-subjects agreement between test and retest, although absolute fractional differences were comparable to those of CBF. Values for washout ($k_2$) and trapping ($k_3$) rate constants (Table 1) were small and highly variable across region, subject and scan. ICC values were high for $k_2$ despite large differences between the test and retest scans (Table 2). This is likely to be due to the even larger variation in $k_2$ values across subjects rather than reflecting strong test-retest repeatability. Test-retest variation in the trapping rate constant $k_3$ was extremely poor (Table 2). Based on estimated parameter errors from the kinetic model fitting, $k_3$ was not significantly greater than zero in 728/780 regions (compared to 11/780 and 337/780 for $K_1$ and $k_2$ respectively). The values obtained for Kmet, PSmet and CMRA showed quite high fractional differences across test and retest scans (Supplement Table 2).

*Model selection:* Considering the ten scans in subjects 1–5, grey matter TAC fits were good for all models with $k_2 > 0$ (Fig. 2). In contrast to the trapping models, a reversible one tissue compartment model (1TCM, $k_3$ & $k_4 = 0$) was the favoured model (majority vote) for grey matter (8/10 scans) and across 74/77 atlas regions (Supplement Fig. 3). Two subjects each had one scan mostly favouring models with $k_3 > 0$, though these were not replicable in the individuals' other scan. Of all 780 TACs (ten scans x 77 ROI and grey matter) 649 (83%) favoured the 1TCM. The repeatability metrics for $K_1$ and $k_2$ calculated using the 1TCM (Table 3) were similar to those calculated using the 2TCM (Table 2). $K_1$ continued to show low or negative ICC values and fractional differences of approximately 10%; $k_2$ showed higher ICC but larger inter-subject variability and test-retest differences.

Table 3

Repeatability metrics for [$^{13}$N]ammonia one tissue compartment (reversible) model parameters for grey matter and selected regions of interest (ROIs). The table presents the intraclass correlation coefficient (ICC), percent mean fractional difference (VAR) and percent absolute fractional difference (AbsVAR) across test (S1) and retest (S2) scans. Data are presented as mean ± standard deviation for grey matter and the left (l) lingual gyrus (OL_ling_G), posterior cingulate gyrus (G_cing_post), putamen, thalamus and cerebellum.

| ROI | K1 [n = 5] (ml/100 g/min) | | | | | k2 [n = 5] (1/min) | | | | |
|---|---|---|---|---|---|---|---|---|---|---|
| | S1 | S2 | ICC | VAR | AbsVAR | S1 | S2 | ICC | VAR | AbsVAR |
| Grey Matter | 20.1 ± 1.5 | 18.6 ± 1.3 | -0.83 | -8 ± 14 | 10 ± 12 | 0.0069 ± 0.0029 | 0.0074 ± 0.0022 | 0.58 | 11 ± 38 | 28 ± 24 |
| OL_ling_G_l | 23.7 ± 3.0 | 21.5 ± 1.0 | -0.41 | -9 ± 15 | 10 ± 14 | 0.0072 ± 0.0023 | 0.0075 ± 0.0020 | 0.58 | 5 ± 30 | 24 ± 15 |
| G_cing_post_l | 22.2 ± 1.6 | 20.6 ± 1.3 | -0.68 | -7 ± 13 | 9 ± 11 | 0.0065 ± 0.0032 | 0.0075 ± 0.0019 | 0.58 | 19 ± 40 | 30 ± 31 |
| Putamen_l | 23.3 ± 1.9 | 21.1 ± 1.5 | -0.83 | -10 ± 15 | 12 ± 12 | 0.0063 ± 0.0028 | 0.0072 ± 0.0028 | 0.59 | 13 ± 44 | 34 ± 27 |
| Thalamus_l | 22.5 ± 2.1 | 20.7 ± 1.1 | -0.79 | -8 ± 15 | 10 ± 13 | 0.0089 ± 0.0030 | 0.0101 ± 0.0024 | 0.72 | 15 ± 23 | 24 ± 9 |
| Cerebellum_l | 22.4 ± 2.0 | 20.6 ± 1.3 | -0.69 | -8 ± 14 | 9 ± 13 | 0.0061 ± 0.0027 | 0.0072 ± 0.0022 | 0.61 | 19 ± 39 | 33 ± 25 |

Finally, the degree to which CBF may have accounted for brain uptake of [$^{13}$N]ammonia was investigated by examining the correlations between [$^{15}$O]water CBF and [$^{13}$N]ammonia $K_1$ (as estimated through irreversible the 2TCM or reversible 1TCM) or $K_{met}$. Correlating within each scan pair (across all ROIs), $K_1$ estimates from 1TCM were most highly correlated with CBF in all 10 scan pairs, with $r^2$ values ranging from 0.72 to 0.92 (Fig. 3). In each of the 10 scan pairs, $r^2$ values were second highest with the 2TCM $K_1$ ($r^2$ between 0.56 to 0.85) and poorest and most variable with $K_{met}$ ($r^2$ between 0.2 to 0.85). However, these strong within-subject correlations were not replicated across subjects within region: no region revealed a significant positive correlation between CBF and $K_1$ or Kmet.

## Discussion

This study evaluated [$^{13}$N]ammonia PET as an *in vivo* method to estimate the rate of conversion of glutamate to glutamine by the enzyme glutamine synthetase (GS) in the human brain. We were able to acquire full datasets comprising two [$^{13}$N]ammonia (test and retest) scans, two [$^{15}$O]water scans and corresponding arterial input functions in five subjects, each on a single day. Kinetic modelling in these subjects was unable to reliably estimate the rate constant relating to GS activity ($k_3$) from that related to [$^{13}$N]ammonia brain uptake ($K_1$) and indicated non-negligible back-flux of [$^{13}$N]ammonia from the brain to the blood. In addition, comparison of K1 estimates with [$^{15}$O]water CBF across brain regions and within-subjects found that these measures were highly correlated and of comparable reliability. Together these results indicate that the

applied [$^{13}$N]ammonia PET method is unable to quantify GS activity in the human brain, and instead may principally index CBF.

Studies in experimental animals have indicated [$^{13}$N]ammonia PET might be able to index GS activity, as irreversible blockade of GS with methionine sulfoximine (MSO) decreases the brain [$^{13}$N]ammonia signal.[34] In kinetic modelling of dynamic [$^{13}$N]ammonia PET images of the human brain, GS activity would be captured by the rate constant $k_3$ in an irreversible two tissue compartment model. Using this model, our analysis returned values for $k_3$ that were highly variable within subjects, as well as between subjects and across grey matter regions. In most instances, $k_3$ values were also too low to be estimated compared to the estimated error. A previous [$^{13}$N]ammonia study in subjects with cirrhosis and healthy volunteers using similar methodology was also unable to provide estimates of $k_3$ [20]. While volume of distribution ($K_1/k_2$) may potentially have provided a surrogate index of GS activity from a reversible model, we were also unable to reliably estimate $k_2$. Overall, this indicates that [$^{13}$N]ammonia PET is unlikely to be a suitable method for measuring the rate of metabolism of glutamate to glutamine by GS in the human brain.

Although the question as to whether ammonia in the brain can diffuse into the blood has previously been debated [35], back-flux of [$^{13}$N]ammonia from brain to blood has now been demonstrated in healthy volunteers as well as subjects with cirrhosis [20, 11, 19]. Similar to these studies, our finding of small but positive values for [$^{13}$N]ammonia $k_2$ also indicate non-zero back-flux of unmetabolized [$^{13}$N]ammonia to blood. Consistent with this, the simplest irreversible model with a single tissue compartment and one rate constant, $K_1$, showed the poorest fit in nearly every dataset. The presence of non-negligible wash-out was also consistent with the plateau of the decay-corrected brain time-activity curves in conjunction with approximately 10% of parent tracer compound remaining in the arterial plasma at the end of the scan. Patlak plots were nonlinear at late times, also indicating the presence of reversibility of the tracer. Our data as well as that of Goldbecker et al. [20] indicate that back-flux of ammonia may be observed (although not reliably quantified) within 30 minutes of [$^{13}$N]ammonia injection. Potential biochemical explanations for washout could include the immediate back-flux of ammonia as well as a longer-term action of glutaminase recycling $^{13}$N from the neuron back to the astrocyte [36].

While our data did not support estimation of GS activity, it did indicate that [$^{13}$N]ammonia PET may provide an index of CBF. [$^{13}$N]ammonia $K_1$ correlated with the $K_1$ (CBF) from the preceding [$^{15}$O]water scans in the same subjects, and based on fractional difference metrics, [$^{13}$N]ammonia brain uptake (K1) was of comparable reproducibility to [$^{15}$O]water CBF measures over the test and retest scanning sessions. The correlations between $K_1$ and CBF were observed when $K_1$ was calculated with either a reversible one-tissue or reversible two-tissue compartment model, and to a lesser extent between $K_i$ (calculated using Patlak analysis) and CBF. The correlations between $K_1$ and CBF were qualitatively tighter for $K_1$ calculated from the one compared to two-tissue compartmental model, as would be expected given there are fewer parameters. Nonetheless the slope of the best fit was not identical between subjects and scans (Fig. 3). Correlating CBF and $K_1$ within region, across subjects and scans, did not yield significant correlation. The source of this variance between subjects and scans is unclear. In rhesus monkeys, Phelps et al. [37] found non-linear relationships between $K_1$ (or specifically extraction fraction, E) and CBF, over a wide range of CBF values. Our data indicate that a linear relationship between $K_1$ and CBF exists when CBF lies within the normal range investigated here.

Compared to the previous study of Keiding and colleagues [11] the values for [$^{13}$N]ammonia $K_1$ obtained in our study are approximately 40% lower. The estimates for permeability-surface area product values and CMRA were similar, while $PS_{met}$ estimates were also slightly lower in our study, which is consistent with lower $K_{met}$ found from the possibly unsuitable graphical method. As in Keiding et al., [11] we applied the Patlak method [32] to calculating $K_{met}$ which avoided replicating the poor identification of $k_2$ and $k_3$ values with an explicit calculation. Nonetheless the fractional differences for $K_{met}$, $PS_{met}$ and CMRA between test and retest scans were high.

One limitation of our study was that full data for plasma time activity curves was unavailable in three of the eight subjects, who were therefore excluded from the main analysis. However, results remained similar when population parent plasma input functions were substituted for these individuals. Repeatability may also have been limited by participant fatigue during the second scanning session, due to the technical complexity of the study and as subjects remained in the PET centre for an average of 3.5 hours between the start of the first scan and end of the last. Although our CBF and $K_1$ ([$^{13}$N]ammonia) values were lower than in Keiding et al [11], inter-subject variances were comparable and the absolute values of CBF were in keeping with the variances seen between centres for quantitative PET studies (e.g. Fan et al [38]). The strong correlations observed between $K_1$ and CBF yielded variable slopes between subjects and scan pairs. It is unclear how much is attributable to a true representation of physiology or to unforeseen errors from the challenges of complex timing with short half-life tracers. GE Discovery 710 PET-CT scanners have a longer scanner bore than the ECAT EXACT HR PET used by Keiding [11] and the necessity of longer arterial lines (150 cm from wrist to detector) may have led to more dispersion of the input function, for both the [$^{13}$N]ammonia and [$^{15}$O]water scans. However, to investigate this further we evaluated an adaption of the Meyer model [27] to the reversible two tissue compartment model, but this yielded the same conclusions and almost identical results, but with increased variability (data not shown).

While the CBF and $K_1$ ([$^{13}$N]ammonia) correlated well within each scan pair, this study did not investigate the quantification or detectability of changes in perfusion *per se*. However, PET tracers with longer radioisotope half-lives are in general easier to incorporate into a scanning schedule and the slower washout of [$^{13}$N]ammonia may yield images with improved signal to noise compared to [$^{15}$O]water. Our results therefore suggest that the use of [$^{13}$N]$NH_3$ as a brain perfusion marker for low to normal blood flow may warrant further investigation.

## Conclusions

Based on our data, cerebral glutamate synthetase activity is not quantifiable using [$^{13}$N]ammonia PET in heathy volunteers. Over a 30-minute uptake period, tissue wash-out of the tracer is identifiable with a simple one-tissue compartmental model, suggesting irreversible models are not strictly appropriate. While the most repeatable uptake parameter, $K_1$, would likely be a macroparameter combining perfusion, PS product and GS activity rather than assessing GS activity per se, it appears to correlate well with CBF and may be useful in this context.

## Declaration

# Ethics approval and consent to participate:

The study had ethical approval from the NHS Ethical Committee (NRES South East Coast, Surrey, Ref: 13/LO/0146), the local Research and Development offices and the Administration of Radioactive Substances Advisory Committee (ARSAC, Certificate RPC 261/3186/29926). All procedures were performed in accordance with the ethical standards of the research committee and with the 1964 Helsinki declaration and its later amendments. Informed consent was obtained from all individual participants included in the study.

# Consent for publication:

Not applicable

# Availability of data and material:

The datasets used and/or analysed during the current study are available from the corresponding author on reasonable request.

# Competing interests:

The authors declare that they have no competing interests.

# Funding:

This work was supported by the Wellcome/EPSRC Centre for Medical Engineering (WT 203148/Z/16/Z) and by the National Institute for Health Research (NIHR) Biomedical Research Centre at South London and Maudsley NHS Foundation Trust and King's College London. The views expressed are those of the authors and not necessarily those of the NHS, the NIHR or the Department of Health and Social Care.

# Authors' contributions:

AE and AG conceptualised and designed the study. The study protocol was developed together with methodological input from JTD, NS, ZY, JO'D, AH, FET and PKM. ZY, JO'D, NS and AG optimised and performed the radiosynthesis and radiometabolite assays and analyses. JTD conducted neuroimaging analyses. ZY and JTD conducted metabolite analyses. NS, AE and IK recruited and screened study participants. IK, JM, and SC were study clinicians. AE, JTD, NS, ZY, FET, PKM, AH and AG interpreted study data. Preparation of the manuscript was led by AE, JTD and NS with contributions from all authors.

# Acknowledgements:

None.

## References

1. Martinez-Hernandez A, Bell KP, Norenberg MD. Glutamine synthetase: glial localization in brain. Science. 1977;195(4284):1356-8. doi:10.1126/science.14400.
2. Eid T, Gruenbaum SE, Dhaher R, Lee TW, Zhou Y, Danbolt NC. The Glutamate-Glutamine Cycle in Epilepsy. Adv Neurobiol. 2016;13:351-400. doi:10.1007/978-3-319-45096-4_14.
3. Rose CF, Verkhratsky A, Parpura V. Astrocyte glutamine synthetase: pivotal in health and disease. Biochem Soc Trans. 2013;41(6):1518-24. doi:10.1042/BST20130237.
4. Eid T, Lee TW, Patrylo P, Zaveri HP. Astrocytes and Glutamine Synthetase in Epileptogenesis. J Neurosci Res. 2019;97(11):1345-62. doi:10.1002/jnr.24267.
5. Haberle J, Gorg B, Toutain A, Rutsch F, Benoist JF, Gelot A et al. Inborn error of amino acid synthesis: human glutamine synthetase deficiency. J Inherit Metab Dis. 2006;29(2-3):352-8. doi:10.1007/s10545-006-0256-5.
6. Spodenkiewicz M, Diez-Fernandez C, Rufenacht V, Gemperle-Britschgi C, Haberle J. Minireview on Glutamine Synthetase Deficiency, an Ultra-Rare Inborn Error of Amino Acid Biosynthesis. Biology (Basel). 2016;5(4). doi:10.3390/biology5040040.
7. Zhou Y, Dhaher R, Parent M, Hu QX, Hassel B, Yee SP et al. Selective deletion of glutamine synthetase in the mouse cerebral cortex induces glial dysfunction and vascular impairment that precede epilepsy and neurodegeneration. Neurochem Int. 2019;123:22-33. doi:10.1016/j.neuint.2018.07.009.
8. Eid T, Thomas MJ, Spencer DD, Runden-Pran E, Lai JC, Malthankar GV et al. Loss of glutamine synthetase in the human epileptogenic hippocampus: possible mechanism for raised extracellular glutamate in mesial temporal lobe epilepsy. Lancet. 2004;363(9402):28-37. doi:10.1016/s0140-6736(03)15166-5.
9. van der Hel WS, Notenboom RG, Bos IW, van Rijen PC, van Veelen CW, de Graan PN. Reduced glutamine synthetase in temporal lobe epilepsy. Neurology. 2005;64(2):326-33.

doi:10.1212/01.WNL.0000149636.44660.99.

10. Benjamin AM, Quastel JH. Metabolism of amino acids and ammonia in rat brain cortex slices in vitro: a possible role of ammonia in brain function. J Neurochem. 1975;25(3):197-206. doi:10.1111/j.1471-4159.1975.tb06953.x.
11. Keiding S, Sorensen M, Bender D, Munk OL, Ott P, Vilstrup H. Brain metabolism of 13N-ammonia during acute hepatic encephalopathy in cirrhosis measured by positron emission tomography. Hepatology. 2006;43(1):42-50. doi:10.1002/hep.21001.
12. Lockwood AH, Bolomey L, Napoleon F. Blood-brain barrier to ammonia in humans. J Cereb Blood Flow Metab. 1984;4(4):516-22. doi:10.1038/jcbfm.1984.76.
13. Lockwood AH, McDonald JM, Reiman RE, Gelbard AS, Laughlin JS, Duffy TE et al. The dynamics of ammonia metabolism in man. Effects of liver disease and hyperammonemia. J Clin Invest. 1979;63(3):449-60. doi:10.1172/JCI109322.
14. Lockwood AH, Yap EW, Wong WH. Cerebral ammonia metabolism in patients with severe liver disease and minimal hepatic encephalopathy. J Cereb Blood Flow Metab. 1991;11(2):337-41. doi:10.1038/jcbfm.1991.67.
15. Ahl B, Weissenborn K, van den Hoff J, Fischer-Wasels D, Kostler H, Hecker H et al. Regional differences in cerebral blood flow and cerebral ammonia metabolism in patients with cirrhosis. Hepatology. 2004;40(1):73-9. doi:10.1002/hep.20290.
16. Weissenborn K, Bokemeyer M, Ahl B, Fischer-Wasels D, Giewekemeyer K, van den Hoff J et al. Functional imaging of the brain in patients with liver cirrhosis. Metab Brain Dis. 2004;19(3-4):269-80.
17. Keiding S, Sorensen M, Munk OL, Bender D. Human (13)N-ammonia PET studies: the importance of measuring (13)N-ammonia metabolites in blood. Metab Brain Dis. 2010;25(1):49-56. doi:10.1007/s11011-010-9181-2.
18. Sorensen M, Keiding S. New findings on cerebral ammonia uptake in HE using functional (13)N-ammonia PET. Metab Brain Dis. 2007;22(3-4):277-84. doi:10.1007/s11011-007-9066-1.
19. Sorensen M, Munk OL, Keiding S. Backflux of ammonia from brain to blood in human subjects with and without hepatic encephalopathy. Metab Brain Dis. 2009;24(1):237-42. doi:10.1007/s11011-008-9126-1.
20. Goldbecker A, Buchert R, Berding G, Bokemeyer M, Lichtinghagen R, Wilke F et al. Blood-brain barrier permeability for ammonia in patients with different grades of liver fibrosis is not different from healthy controls. J Cereb Blood Flow Metab. 2010;30(7):1384-93. doi:10.1038/jcbfm.2010.22.
21. He Q, Zhang L, Zhang B, Shi X, Yi C, Zhang X. Diagnostic accuracy of (13)N-ammonia PET, (11)C-methionine PET and (18)F-fluorodeoxyglucose PET: a comparative study in patients with suspected cerebral glioma. BMC Cancer. 2019;19(1):332. doi:10.1186/s12885-019-5560-1.
22. Wieland B, Bida G, Padgett H, Hendry G, Zippi E, Kabalka G et al. In-Target Production of [N-13] Ammonia Via Proton Irradiation of Dilute Aqueous Ethanol and Acetic-Acid Mixtures. Appl Radiat Isotopes. 1991;42(11):1095-8.
23. Berridge MS, Terris AH, Cassidy EH. Low-Carrier Production of [O-15] Oxygen, Water and Carbon-Monoxide. Appl Radiat Isotopes. 1990;41(12):1173-5.
24. Gousias IS, Rueckert D, Heckemann RA, Dyet LE, Boardman JP, Edwards AD et al. Automatic segmentation of brain MRIs of 2-year-olds into 83 regions of interest. Neuroimage. 2008;40(2):672-84. doi:10.1016/j.neuroimage.2007.11.034.
25. Hammers A, Allom R, Koepp MJ, Free SL, Myers R, Lemieux L et al. Three-dimensional maximum probability atlas of the human brain, with particular reference to the temporal lobe. Hum Brain Mapp. 2003;19(4):224-47. doi:10.1002/hbm.10123.
26. Ashburner J, Friston KJ. Unified segmentation. Neuroimage. 2005;26(3):839-51. doi:10.1016/j.neuroimage.2005.02.018.
27. Meyer E. Simultaneous correction for tracer arrival delay and dispersion in CBF measurements by the H215O autoradiographic method and dynamic PET. J Nucl Med. 1989;30(6):1069-78.
28. DeGrado TR, Hanson MW, Turkington TG, Delong DM, Brezinski DA, Vallee JP et al. Estimation of myocardial blood flow for longitudinal studies with 13N-labeled ammonia and positron emission tomography. J Nucl Cardiol. 1996;3(6 Pt 1):494-507.

29. Cooper AJ, McDonald JM, Gelbard AS, Gledhill RF, Duffy TE. The metabolic fate of 13N-labeled ammonia in rat brain. J Biol Chem. 1979;254(12):4982-92.
30. Veronese M, Rizzo G, Bertoldo A, Turkheimer FE. Spectral Analysis of Dynamic PET Studies: A Review of 20 Years of Method Developments and Applications. Comput Math Methods Med. 2016;2016:7187541. doi:10.1155/2016/7187541.
31. Akaike H. Likelihood of a Model and Information Criteria. J Econometrics. 1981;16(1):3-14. doi:Doi 10.1016/0304-4076(81)90071-3.
32. Patlak CS, Blasberg RG, Fenstermacher JD. Graphical evaluation of blood-to-brain transfer constants from multiple-time uptake data. J Cereb Blood Flow Metab. 1983;3(1):1-7. doi:10.1038/jcbfm.1983.1.
33. McGraw KO, Wong SP. Forming inferences about some intraclass correlation coefficients. Psychol Methods. 1996;1(1):30-46. doi:Doi 10.1037/1082-989x.1.1.30.
34. Momosaki S, Ito M, Tonomura M, Abe K. Assessment of glutamine synthetase activity by [13N]ammonia uptake in living rat brain. Synapse. 2015;69(1):26-32. doi:10.1002/syn.21781.
35. Ott P, Larsen FS. Blood-brain barrier permeability to ammonia in liver failure: a critical reappraisal. Neurochem Int. 2004;44(4):185-98.
36. Cooper AJ. 13N as a tracer for studying glutamate metabolism. Neurochem Int. 2011;59(4):456-64. doi:10.1016/j.neuint.2010.11.011.
37. Phelps ME, Huang SC, Hoffman EJ, Selin C, Kuhl DE. Cerebral extraction of N-13 ammonia: its dependence on cerebral blood flow and capillary permeability – surface area product. Stroke. 1981;12(5):607-19. doi:10.1161/01.str.12.5.607.
38. Fan AP, Jahanian H, Holdsworth SJ, Zaharchuk G. Comparison of cerebral blood flow measurement with [15O]-water positron emission tomography and arterial spin labeling magnetic resonance imaging: A systematic review. J Cereb Blood Flow Metab. 2016;36(5):842-61. doi:10.1177/0271678X16636393.

## Figures

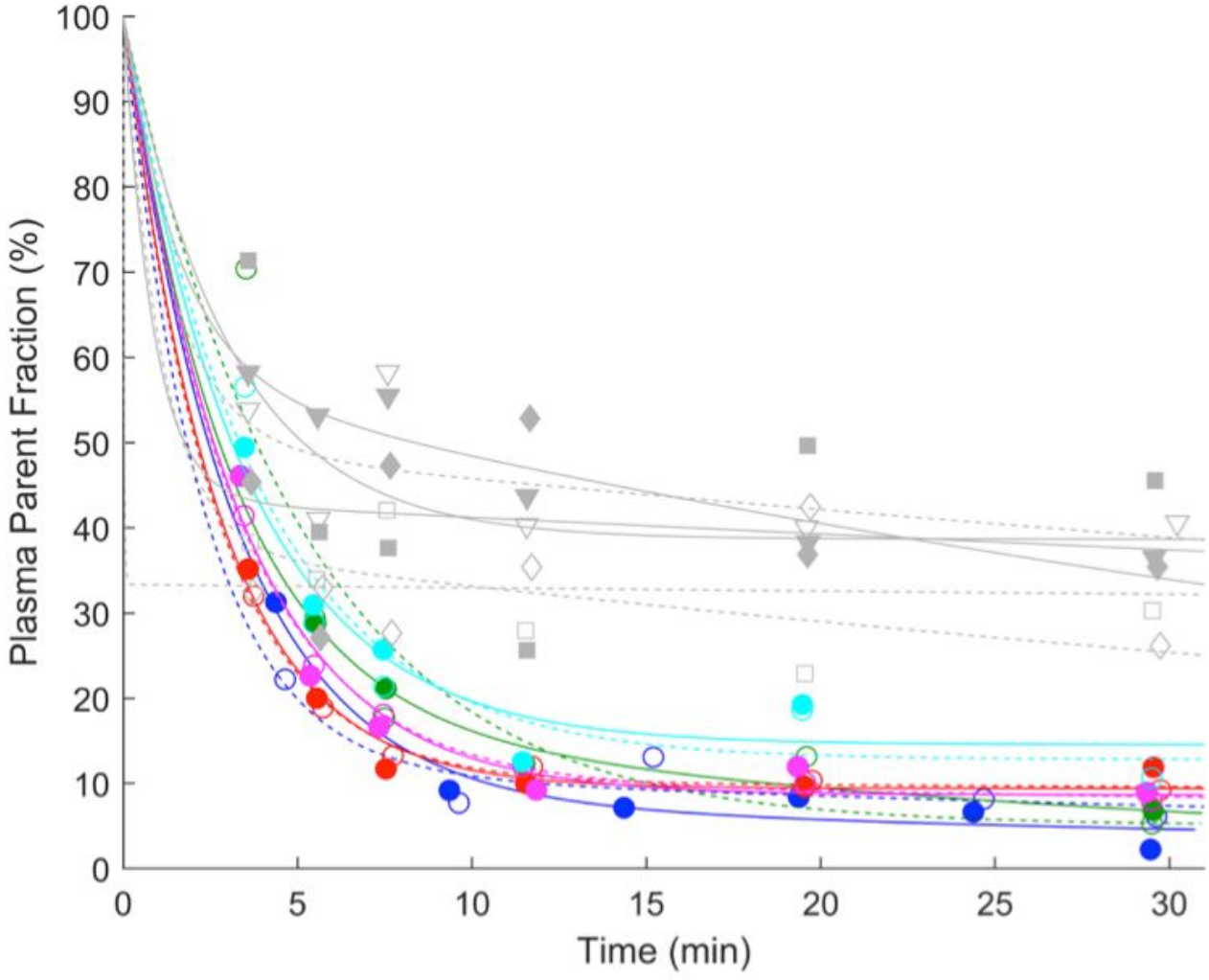


**Figure 1**

Plasma parent fraction data & fit Symbols represent ratio of parent compound, [13N]NH3, to 13N labelled metabolites measured in individual arterial plasma samples. Lines show biexponential fits to subject/scan data sets. Coloured lines and circles show colour-coded subjects 1-5 used in the full analysis. Grey lines and symbols (coded by subject) show subjects 6-8 treated as corrupted data. Solid line and filled symbols show data from scan 1, dashed lines and open symbols from scan 2. X-axis is time in minutes from injection (corrected for brain-detector delay). Y-axis is plasma parent fraction in percent.

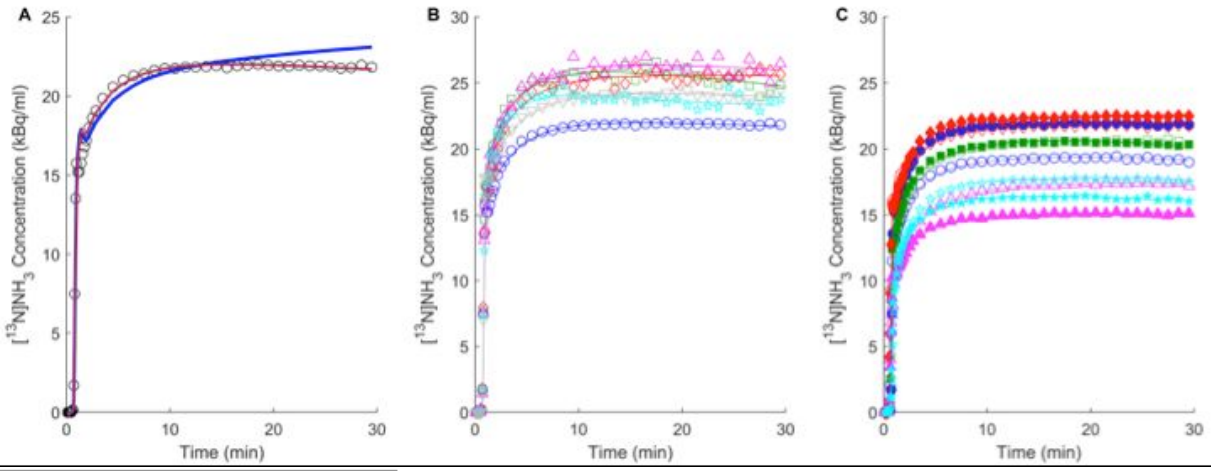

**Figure 2**

Ammonia TAC data & fits Symbols show example time activity curves (TACs) from ammonia PET scans and lines show model fits. A: blue line: irreversible 1TCM (K1 plus blood volume, Vb); green line: reversible 1TCM (K1, k2, Vb); red line: irreversible 2TCM (K1, k2, k3, Vb) and magenta line: reversible 2TCM (K1, k2, k3, k4, Vb). The most complex three models appear to fit equally well and appear as superimposed on the graph. B: TAC and irreversible 2TCM model fits from subject 1 for grey matter (circle), left lingual gyrus (square), left posterior cingulate gyrus (diamond), left putamen (up triangle), left thalamus (star) and left cerebellum (down triangle). C: TACs and irreversible 2TCM model fits for grey matter in subjects 1-5. Solid symbols and solid lines show scan 1, open symbols and dashed lines scan 2.

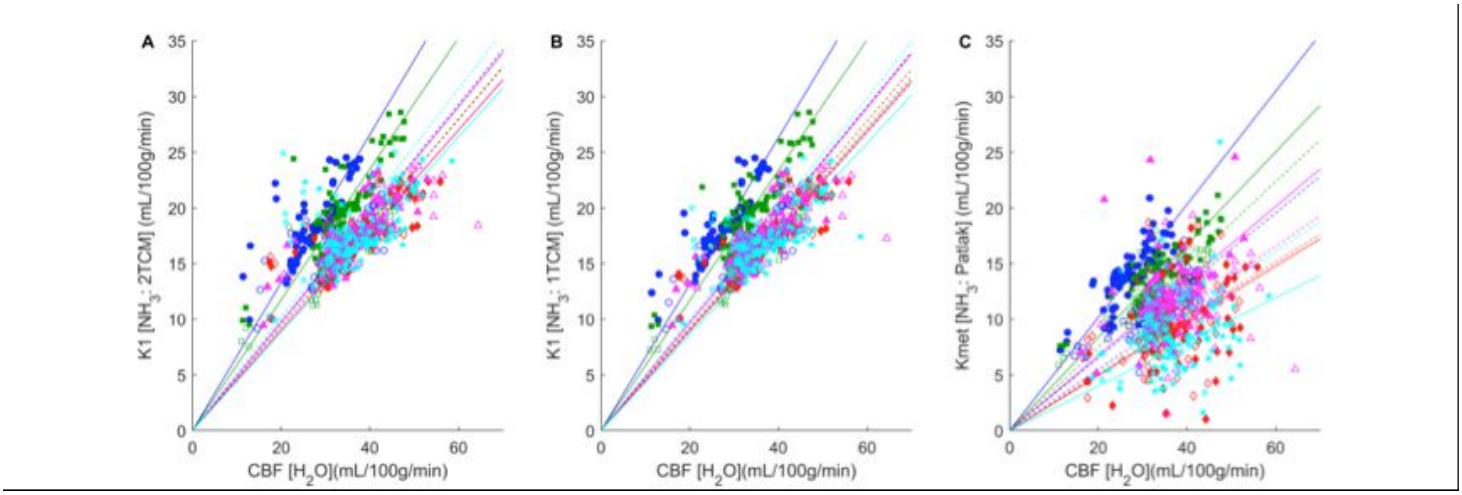


**Figure 3**

CBF vs K1 correlations Plots showing association across 78 ROIs of K1 (y-axis)from model fits of [13N]NH3 data with CBF (x-axis) from paired [15O]H2O scans within each subject (1-5) and for scans 1 & 2. Lines show line of best fit (zero intercept). Subjects 1-5 are coded with symbol type and colour. Solid symbols and solid lines show scan 1, open symbols and dashed lines scan 2. A: K1 calculated from irreversible 2TCM; B: K1 calculated from reversible 1TCM; C: Kmet calculated from Patlak plot. CBF is calculated using the Meyer[27] model described in the manuscript.

## Supplementary Files

This is a list of supplementary files associated with this preprint. Click to download.

- AmmoniaPETSupplementaryInformation24APR20final.docx